

## Analysis of the collision-damage susceptibility of sweet cherry related to environment temperature: A numerical simulating method

Item Type	Journal article
Authors	Han, Xuewei;Liu, Ying;Tchuenbou-Magaia, Fideline Laure;Li, Zhiguo;Khojastehpour, Mehdi;Li, Bangxin
Citation	Han, X., Liu, Y., Tchuenbou-Magaia, F., Li, Z., Khojastehpour, M. and Li, B. (2022) Analysis of the collision-damage susceptibility of sweet cherry related to environment temperature: A numerical simulating method. Journal of Food Engineering, 333, 111140.
DOI	<a href="https://doi.org/10.1016/j.jfoodeng.2022.111140">10.1016/j.jfoodeng.2022.111140</a>
Publisher	Elsevier
Journal	Journal of Food Engineering
Download date	2026-03-17 03:41:28
License	<a href="https://creativecommons.org/licenses/by-nc-nd/4.0/">https://creativecommons.org/licenses/by-nc-nd/4.0/</a>
Link to Item	<a href="http://hdl.handle.net/2436/624775">http://hdl.handle.net/2436/624775</a>

# Analysis of the collision-damage susceptibility of sweet cherry related to environment temperature: A numerical simulating method

Xuewei Han<sup>a</sup>, Ying Liu<sup>a</sup>, Fidelity Tchuenbou-Magaia<sup>b</sup>, Zhiguo Li<sup>a,\*</sup>, Mehdi Khojastehpour<sup>c</sup>, Bangxin Li<sup>d,\*</sup>

<sup>a</sup>College of Mechanical and Electronic Engineering, Northwest A&F University, Yangling, 712100, China

<sup>b</sup>School of Engineering, Computing and Mathematical Sciences, Division of Chemical Engineering, University of Wolverhampton, Wolverhampton, WV1 1LY, UK

<sup>c</sup>Department of Biosystems Engineering, Ferdowsi University of Mashhad, Mashhad, Iran

<sup>d</sup>School of Automation and Electrical Engineering, Lanzhou Jiaotong University, Lanzhou 730070, China

\*Correspondence Email: lizhiguo0821@163.com (Z. Li)

**Abstract:** Sweet cherry is extremely susceptible to collision damage during post-harvest handling which results in increased fruit waste and low fruit economic value. Fruit-to-rigid surface and fruit-to-fruit collision systems were modeled by the dynamic FE method and the sweet cherry model included three parts: exocarp, mesocarp, and pit. A fruit-to-rigid surface horizontal collision testbed was newly developed to validate the prediction accuracy of the fruit FE model. It was found that the fruit model inputting the average elastic moduli and failure stress of the fruit tissues can reproduce the experimental maximum impact force and contact time in the compression stage with the relative error of 1.58 and 1.87 %, respectively. Three mathematical models were proven to be capable of quantitatively assessing the internal damage degree of sweet cherry by three independent variables: collision type, initial fruit velocity, and environment temperature. This study shows an effective numerical simulation approach for objectively predicting the horizontal collision-damage susceptibility of sweet cherry. The principle can be applied to other fruits and thus pave the way for improving tools/equipment and the creation of appropriate conditions for fruit picking, grading, packaging, and transportation to support the actualization of waste reduction and sustainable food systems.

**Keywords:** Sweet cherry; Collision; Temperature effect; Damage susceptibility; Finite element analysis

Nomenclature			
$CT$	collision type, $CT = 0$ means fruit-to-rigid surface collision, and $CT = 1$ means fruit-to-fruit collision	$t_0$	time corresponding to start frame, ms
$E_{ex}$	elastic modulus of exocarp, MPa	$t_1$	time corresponding to tagged frame, ms
$E_{me}$	elastic modulus of mesocarp, MPa	$V_{fd}$	fruit damage volume, mm <sup>3</sup>
$E_p$	elastic modulus of pit, MPa	$V_f$	fruit geometric volume, mm <sup>3</sup>
$E_{tex}$	tangent modulus of exocarp, MPa	$V_{ex}$	damage volume of exocarp, mm <sup>3</sup>
$E_{tme}$	tangent modulus of mesocarp, MPa	$V_{me}$	damage volume of mesocarp, mm <sup>3</sup>
$F_{max}$	maximum impact force, N	$v$	initial fruit velocity, m/s
$L_{ex}$	side length of exocarp element, mm	$\epsilon_{ex}$	plastic strain of exocarp
$L_{me}$	side length of mesocarp element, mm	$\epsilon_{me}$	plastic strain of mesocarp
$N_{ex}$	number of failure integration points in all exocarp elements	$\nu_{ex}$	Poisson's ratio of exocarp
$N_{me}$	number of failure integration points in all mesocarp elements	$\nu_{me}$	Poisson's ratio of mesocarp
$P_{fd}$	percentage of damage volume for whole fruit, %	$\nu_p$	Poisson's ratio of pit
$P_{ex}$	percentage of exocarp damage volume, %	$\rho_{ex}$	density of exocarp, g/cm <sup>3</sup>
$P_{me}$	percentage of mesocarp damage volume, %	$\rho_{me}$	density of mesocarp, g/cm <sup>3</sup>

$R$	curvature radius of contact point at fruit surface, mm	$\rho_p$	density of pit, g/cm <sup>3</sup>
$S_f$	horizontal moving displacement of fruit for the duration ( $t_1 - t_0$ ), mm	$\sigma_{ex}$	failure stress of exocarp, MPa
$T$	environment temperature, °C	$\sigma_{max}$	maximum Von mises stress of fruit model, MPa
$T_c$	contact time in compression stage, ms	$\sigma_{me}$	failure stress of mesocarp, MPa

## 23 1. Introduction

24 Sweet cherry has a soft texture and is easy to be damaged (Pullanagari and Li, 2021). In the process of  
25 picking, sorting, packaging and transportation, there are often collisions between fruit and fruit, and between  
26 fruit and rigid surface, resulting in a dynamic mechanical damage which seriously affect fruit economic value  
27 (Michailidis et al., 2019; Wang et al., 2020). When sweet cherry is subjected to mechanical impact, the cells  
28 in the damaged area were destroyed (Yousefi et al., 2016), and the cell wall was subsequently decomposed  
29 under the catalysis of enzymes, causing bruising in the damaged area (An et al., 2022). This bruising causes  
30 sweet cherry to become less resistant to microbial invasion, thereby accelerating the decay process, and the  
31 loss of their commercial value (Gu et al., 2022). Sweet cherry is always exposed to a wide range of  
32 environmental temperatures (approximately 0 to 40 °C) during various post-processing operations (including  
33 picking, grading, packaging, transportation, and sales) (Yamazaki and Hosokawa, 2019; Zhao et al., 2021).  
34 From a material mechanics point of view, environmental temperature conditions are one of the environmental  
35 factors which have the most influence on the material properties. Different environment temperatures can alter  
36 enzymes' activity, pectin and cellulose viscosity, and water content in pulp cells (Karatas and Arslan, 2016).  
37 For example, higher environment temperature can accelerate cellular enzymatic reactions, which is evidenced  
38 macroscopically by a reduction in the fruit firmness (Brüggenwirth and Knoche, 2016). Therefore, it is of great  
39 significance to study the dynamic impact damage of sweet cherry related to environmental temperature.

40 Previous studies can be divided into two aspects, namely, the factors affecting the sweet cherry damage  
41 source and the effect of low-temperature storage on the changes of nutrient composition and texture of sweet  
42 cherry. Brueggenwirth et al. (2014) proposed that the sweet cherry skin was isotropic and its mechanics mainly  
43 depended on the epidermis and hypodermis but not the cuticle. Zhou et al. (2016a and 2016b) found that the  
44 sweet cherry was more easily damaged at the vibration frequency of 18 Hz when compared to vibration  
45 frequencies of 10 Hz and 14 Hz, and the damage rate was as high as 35 %. Alique et al. (2005) investigated  
46 the effects of three pretreatment methods of water cooling, natural cooling, and hot water treatment on the  
47 texture mechanics of sweet cherry and found that hot water treatment reduced the hardness of sweet cherry  
48 from  $9.1 \pm 0.6$  N to  $6.2 \pm 0.4$  N while accelerating the ripening which led to rapid consumption of glucose and  
49 malic acid as well as an increase in the fruit softness. Wang and Long (2014) proposed that the firmness of two

50 sweet cherry varieties increased by 21 % ~ 42 % after being stored in modified atmosphere packaging at 0 °C  
51 for 6 weeks. Brüggewirth and Knoche (2016) proposed that with the increase in temperature the failure stress  
52 and elastic modulus of sweet cherry skins decreased. Zhao et al. (2019) concluded that the storage at near-  
53 freezing temperature can effectively delay the ripening process of sweet cherry fruit, evidenced by a prolonged  
54 storage time, decrease in the fruit softening rate, and reduction of the decomposition of anthocyanin and sugar  
55 content whilst maintaining its skin color.

56 In summary, the existing literature shows that great progress has been made in characterizing sweet cherry  
57 mechanical damage and the texture change in post-harvest at relatively low-temperature storage. Moreover, it  
58 is well established that the finite element (FE) method is a powerful numerical prediction technique for solving  
59 complex mechanical damage problems of fruit and vegetable subjected to an external force, and has been used  
60 as an alternative to providing additional insights that are often impractical or impossible to achieve through  
61 real-world experimental or to complement real-world experimentation. For example, researchers have  
62 investigated the mechanical damage phenomena of apple (Ahmadi et al., 2016), pear (Salarikia et al., 2017),  
63 kiwifruit (Du et al., 2019), grape (Miraei Ashtiani et al., 2019), orange (Namdari Gharaghani et al., 2018) and  
64 potato (Nikara et al., 2020) using nonlinear FE method. However, there are few reports about the dynamic  
65 impact damage of sweet cherry during postharvest packaging and transportation at different environment  
66 temperatures. In consideration that sweet cherry is always exposed to a wide range of environmental  
67 temperatures (about 0 to 40 °C) during picking, grading, packaging, transportation, and sales (Yamazaki and  
68 Hosokawa, 2019; Zhao et al., 2021), the gap not only limits the prediction of the level of collision damage of  
69 the fruit under a specific temperature at post-processing stages, but also hampers theoretical guidance for the  
70 development and working environment of sweet cherry picking, grading, packaging and transportation  
71 equipment. Sweet cherry fruit has elastic-plastic mechanical characteristics, and its dynamic collision process  
72 is an extremely complex nonlinear dynamic behavior (Zulkifli et al., 2020). Compared with the static  
73 mechanics process, the dynamic collision is accompanied by a high speed and high energy whilst the action  
74 time is short, and the impact force changes rapidly, which results in a large deformation and failure damage in  
75 the local fruit tissue participating in dynamic collision at the moment of impact (Celik et al., 2011; Pieczywek  
76 and Zdunek, 2014). In the explicit FE method, the central difference integration operator is explicit in that the  
77 kinematic state can be advanced using the kinematic parameters (velocity and acceleration) from the previous  
78 increment. This method integrates through time by using many small time increments and the use of diagonal  
79 element mass matrices improves the computational efficiency of the explicit procedure, thereby making it

80 suitable for solving the dynamic collision process of sweet cherry (Wu and Gu, 2012). Furthermore, the damage  
81 evolution process of the sweet cherry during dynamic collision can be visually studied when the tissue failure  
82 stress threshold determined through an experimental process is used for obtaining those parameters such as  
83 damage volume and energy change in post-processing analysis, which is difficult to be achieved by real  
84 experimental method (Li et al., 2013). Therefore, the purpose of this study was to explore a method that could  
85 be used to quantitatively analyze the dynamic collision-damage susceptibility of sweet cherry under different  
86 environmental temperatures during postharvest mechanical handlings.

## 87 **2. Materials and methods**

### 88 **2.1 3D virtual finite element modeling of sweet cherry collision system**

89 *Geometric modeling:* Firstly, a sweet cherry was cut into two 1/2 bodies along the longitudinal equatorial  
90 section with a sharp biological thin cutter, followed by a cut of the seedless 1/2 sweet cherry into 1/4 bodies  
91 along the stem-blossom axis (Fig. 1A). A digital camera was used to take pictures of the two cut surfaces on  
92 the 1/4 sweet cherry, and then two photos were imported into the front-view reference plane and the right-view  
93 reference plane in the sketch drawing area of the SolidWorks software (Version: 2021, Dassault Systemes  
94 Simulia Corp., USA), respectively. Subsequently, the boundary contour closed spline on each of the two cut-  
95 surface views of the 1/4 sweet cherry was sketched (Fig. 1A) and the 1/4 mesocarp geometric model was  
96 created through some operation commands such as filled surface and lofted boss/base. Using the above similar  
97 method, the left three blocks of 1/4 mesocarp tissue were geometrically modeled and then all the 1/4 mesocarp  
98 geometric models were combined into a single mesocarp geometric model. Similarly, the geometric models of  
99 the whole exocarp and pit were created based on the average exocarp thickness of 0.29 mm measured by Han  
100 et al. (2022) and the outer contour curve of the pit. Subsequently, a 2D square discrete rigid body (side length:  
101 60 mm) was created in the Abaqus software (Version: 2020, Dassault Systemes Simulia Corp., USA) as the  
102 rigid surface for collision, and the exocarp, mesocarp and pit geometric models were imported into the Abaqus  
103 for assembling a sweet cheery geometric model (Fig. 1A). Lastly, the geometric models of the fruit-to-rigid  
104 surface and fruit-to-fruit collision systems were constructed, respectively.

105 *Interaction definition:* For the geometric model of the fruit-to-rigid surface horizontal collision system,  
106 the elastic modulus of exocarp was always greater than of mesocarp in sweet cherry (Han et al., 2022).  
107 Therefore, when the interaction between exocarp and mesocarp in a real sweet cherry was simulated by the tie  
108 constraint, the inner surface of the exocarp model was defined as a master surface while the outer surface of  
109 the mesocarp model was defined as a slave surface. Similarly, the outer surface of the pit model was defined

110 as a master surface while the inner surface of the mesocarp model was defined as a slave surface for simulating  
111 the interaction between mesocarp and pit in a real sweet cherry. It is important to ensure that the motion and  
112 stress values of common nodes on the master surface and the slave surface of the binding area in a contact pair  
113 are the same. The interaction between the sweet cherry and the rigid surface in the fruit-to-rigid surface  
114 collision system was defined as general contact (Explicit). In the real world, the physical process of the  
115 collision between the fruit and the rigid surface does not produce mutual penetration between the two contact  
116 surfaces, so the normal behavior of the contact property was defined as hard contact, and the general contact  
117 algorithm prevents contact penetration of nodes on the fruit model surface into the rigid surface by generating  
118 contact forces. The tangential behavior was set to obey Coulomb's friction law, and the penalty function friction  
119 formula was used to simulate the tangential friction behavior between the fruit surface and rigid surface. A  
120 similar approach defines generic contact interactions among the components of the geometric model of the  
121 fruit-to-fruit horizontal collision system.

122 *Boundary conditions and meshing:* For the geometric model of the fruit-to-rigid surface horizontal  
123 collision system, the rigid surface was relatively stationary during the collision process, so the rigid surface  
124 was fixed to remove all degrees of freedom. For the geometric model of the fruit-to-fruit horizontal collision  
125 system, the two fruits move towards each other during the collision process, thus, no boundary conditions were  
126 set for the two fruits. It is very important to select appropriate elements for the finite element model, which  
127 directly affects the accuracy and duration of finite element calculations. The second-order tetrahedral elements  
128 were used for this simulation, which can easily realize the local element refinement of the model, as well as  
129 conveniently capture the position of high stress gradient and reduce the complex meshing process whilst being  
130 suitable for irregular fruit tissue model (Miraei Ashtiani et al., 2019). Considering that the mesh density will  
131 influence the solution accuracy and computer time (Celik et al., 2017), some simple simulations with several  
132 element sizes (e.g., 0.8, 1 and 1.5 mm) were performed for the mesh sensitivity check. Hence, the exocarp,  
133 mesocarp, and pit model were meshed into 10-node modified quadratic tetrahedral elements (C3D10M) with  
134 the global size of 1 mm, and then the exocarp, mesocarp, and pit were meshed into 30230, 85641 and 8533  
135 elements, respectively. The rigid surface was meshed into 3600 elements using R3D4 discrete rigid body  
136 elements. Finally, a fruit-to-rigid surface horizontal collision finite element model and a fruit-to-fruit horizontal  
137 collision finite element model were created, as shown in Fig. 1B.

138 *Assumption:* In order to simplify the collision calculation problem of this dynamic finite element model,  
139 the simulation process follows the following assumptions: (1) The exocarp and mesocarp tissues of sweet

140 cherry were regarded as isotropic and homogeneous elastic-plastic biomaterials whereas the pit was considered  
141 as a linear elastic material. In this study, the bilinear isotropic hardening model was used as the constitutive  
142 model of the elastic-plastic exocarp and mesocarp tissue material, which followed the isotropic hardening law.  
143 When the tissue material exceeds its failure stress, plastic deformation occurs, and the stress of the tissue  
144 material is a function of its plastic strain. In addition, since the elastic modulus of the sweet cherry pit is much  
145 larger than that of the exocarp and the mesocarp, almost no deformation occurs during the collision process,  
146 thus the pit was set as a linear elastic material model. (2) The biological yield point of the sweet cherry tissue  
147 specimen is regarded as the initial point of tissue plastic failure. At the beginning of loading, the tissue material  
148 exhibits linear elastic behavior, and as the load increases to the initial point of tissue plastic failure, the  
149 relationship between the stress and strain of the tissue material exhibits a plastic deformation process. At this  
150 point, the tissue material begins to produce permanent deformation, and after unloading, the tissue material  
151 cannot return to its original state. Therefore, the biological yield point of the sweet cherry tissue was defined  
152 as the initial point of plastic failure, and was used to determine whether the sweet cherry tissue will suffer  
153 impact damage during a horizontal collision (Celik, 2017). (3) The damage behavior of sweet cherry tissue  
154 was predicted by Von mises stress failure criterion (Miraei Ashtiani et al., 2019). The Von mises equivalent  
155 stress follows the maximum distortion-energy theory of material mechanics. In biomechanical calculations, it  
156 is feasible to use the measured tissue material parameters to calculate the von mises stress distribution inside  
157 the tissue for predicting the tissue damage behavior.

## 158 **2.2 Validation of the fruit finite element model**

159 In order to select the most accurate 3D sweet cherry FE model for the following horizontal-collision  
160 simulation and damage prediction analysis, a horizontal collision experiment between sweet cherry fruit and  
161 rigid surface was performed at room temperature, and then the minimum, average and maximum elastic  
162 modulus and failure stress of the fruit exocarp and mesocarp were inputted into the above established sweet  
163 cherry FE model for simulating the real horizontal collision experiment, respectively. Lastly, the results of the  
164 experiment and the simulation (Fig. 1C), such as the maximum impact force during the fruit collision process  
165 and the contact time during the compression stage (Fig. 1D), were compared.

166 *Experimental method for horizontal collision between sweet cherry fruit and rigid surface:* Firstly, a fruit-  
167 to-rigid surface horizontal collision test device (Fig. 2A) was self-developed. This is mainly composed of an  
168 ejection device, a high-speed camera system, a force data acquisition system and a power supply system. The  
169 ejection device has an ejection rod, an ejection tube, a pushbutton, an ejection mouth, a rigid pad, a spring and

170 a support base. The high-speed camera system includes a high-speed camera (DSC-RX100M4, Sony China  
171 Co., Ltd., China) and a camera mount. The force data acquisition system includes a rigid surface, a base, a  
172 translation platform, a ruler, a force sensor (JHBM-H1, Bengbu Sensor System Engineering Co., Ltd., China),  
173 an amplifier, a data acquisition card (USB3100N, Beijing Art Technology Development Co., Ltd., China) and  
174 a computer. The amplifier, the data acquisition card, and the transformer are integrated into the control box. A  
175 USB data cable was used to connect the data acquisition card to the computer for the acquisition of force-time  
176 data during the horizontal collision between the sweet cherry fruit and the rigid surface. Note that the force  
177 sensor should be calibrated to determine a linear function of force and voltage signal before using the device.  
178 Secondly, during the experiment, the ejection rod was pulled backward to make the pushbutton embedded in  
179 the slot of the ejection rod. At this time, the spring inside the ejection tube was in a compressed state. The  
180 cylinder at the rear end of the rigid pad was installed into the end of the ejection tube. Make sure that the flower  
181 stem axis of sweet cherry in the ejection mouth coincides with the axis of the ejection rod and the rigid pad,  
182 keeping it perpendicular to the rigid surface. The camera position was adjusted so that the lens was 20 cm  
183 above the line between the ejection mouth and the rigid surface. The focal length of the camera was adjusted  
184 to ensure that the field of view was large enough and the scale of the ruler was clear. The camera was set to  
185 high frame rate (HFR) mode (capture rate is 1000 frames/second). After pressing the camera record button, the  
186 computer operated to start recording the force sensor data, then the pushbutton was pulled quickly and the  
187 ejection rod in the ejection device impacted the ejection pad forward, then the ejection pad impacted the sweet  
188 cherry fruit. Finally, the obtained impact energy of sweet cherry was converted into kinetic energy and the  
189 sweet cherry moved horizontally, collided with the rigid surface installed on the force sensor. The force sensor  
190 recorded the impact force-time data between the fruit and the rigid surface in real-time during the collision  
191 process and transmitted it to the computer through the amplifier and USB3100N data acquisition card for  
192 storage. The whole process of the horizontal collision between the sweet cherry fruit and the rigid surface was  
193 also recorded synchronously in real-time by a high-speed camera (Fig. 2B). The horizontal collision process  
194 between the sweet cherry fruit and the rigid surface includes the compression and recovery stages. After the  
195 real experiment in this section, the maximum impact force and the contact time in the compression stage were  
196 extracted.

197 In addition, in order to obtain the fruit initial velocity  $v$  during the horizontal collision between the sweet  
198 cherry fruit and the rigid surface, the Adobe After Effects software (Version: 2020, Adobe Systems  
199 Incorporated, USA) was used to process the sweet cherry motion video captured by the high-speed camera.

200 The video frame at the ejection mouth was recorded as the start frame, and the corresponding moment is  
201 recorded as  $t_0$ ; the 20<sup>th</sup> frame after the start frame was recorded as the marked frame extracted during the  
202 horizontal movement of the sweet cherry with corresponding time was recorded as  $t_1$ . This period of time was  
203 denoted as  $\Delta T = t_1 - t_0$ , and the horizontal movement displacement of the sweet cherry during this period is  
204 denoted as  $S_f$ . Therefore, the average horizontal movement velocity of sweet cherry can be calculated by  
205 Equation (1). Considering that the moving distance of the fruit from the ejection mouth to the rigid plate was  
206 short, and ignored the air resistance, this calculated velocity can be regarded as the average initial velocity  $v$   
207 of the horizontal collision between the sweet cherry fruit and the rigid surface. In order to minimize the  
208 difference in mass and shape among different sweet cherry individuals, seven individual sweet cherries with  
209 similar mass and shape were selected to complete seven experiments. The average velocity of the seven  
210 experiments was recorded as the initial velocity of the fruit colliding with the rigid surface during the  
211 simulation of the subsequent validation experiment.

$$212 \quad v = \frac{S_f}{t_1 - t_0} \quad (1)$$

213 *Simulation method of horizontal collision between sweet cherry fruit and rigid surface:* According to the  
214 FE model of the 3D collision system created in Section 2.1, the average velocity of the above seven  
215 experiments was set as the initial velocity of sweet cherry during the simulation in this section. The elastic  
216 modulus and failure stress of the exocarp and mesocarp of sweet cherry fruit at room temperature (20 °C) were  
217 set to the maximum average and minimum values of the measured values reported by Han et al. (2022),  
218 respectively. Other parameters of the fruit model were set to the value from the literature (He and Shi, 2009;  
219 Du et al., 2019; Mahiuddin et al., 2020) (See Table 1). There were three simulations for the horizontal collision  
220 process between the fruit and the rigid surface. Because the fruit material showed a nearly elastic-plastic  
221 behavior during testing, the collision process was regarded as an inelastic collision, and the impact process  
222 included two stages of compression and recovery (Li et al., 2017). During fruit collision with the rigid surface,  
223 the impact force on the rigid surface changed with contact time at the contact point. After the simulation, the  
224 internal stress distribution change process of the fruit tissue during the collision process was extracted. The  
225 maximum support reaction force subjected by the rigid surface was taken as the maximum impact force  $F_{\max}$   
226 of the fruit impacting on the rigid surface during the collision whereas the time taken by the support reaction  
227 force rising from 0 (just contact) to the maximum impact force  $F_{\max}$  was recorded as the contact time in the  
228 compression stage  $T_c$ .

### 229 **2.3 Loading and simulation**

230 The most accurate FE model of sweet cherry fruit verified in Section 2.2 was used for this horizontal  
231 collision simulation. The collision damage of sweet cherry fruit often occurs in the post-harvest processing  
232 process whose environmental temperature often fluctuates between 0 and 40 °C, and collision may occur  
233 between the fruit and the rigid surface, and between the fruit and the fruit. The initial velocity of the fruit before  
234 impact may be different, depending on the external vibration conditions. Therefore, in this paper three initial  
235 fruit velocities (1 m/s, 2 m/s, 3 m/s), three environmental temperatures (5 °C, 20 °C, 40 °C), and two different  
236 collision types (fruit-to-rigid surface, fruit-to-fruit) were considered. To compare the collision process of two  
237 collision types: fruit-to-rigid surface and fruit-to-fruit, considering that two fruits move toward each other for  
238 fruit-to-fruit collision type when they collide with each other and the consistency of the collision velocity  
239 between the two objects should be ensured for two collision types, so the initial velocity of fruit in the fruit-  
240 to-fruit collision type was set to its half in the fruit-to-rigid surface collision type.

241 During the simulation, the mechanical parameters of the exocarp and mesocarp tissue at the corresponding  
242 temperature were input into the FE model to replace the effect of different temperature fluctuations in Table 1  
243 (Han et al., 2022). The Poisson's ratio of sweet cherry exocarp and mesocarp was set based on the existing  
244 literature of Mahiuddin et al. (2020). An automatic density measuring instrument (MH-300A, Xiamen Fubusi  
245 Testing Equipment Co., Ltd., China) was used to measure the density of sweet cherry exocarp, mesocarp and  
246 pit; with reference to the mechanics of walnut shells (He and Shi, 2009) as these parameters were used to set  
247 the elastic modulus and Poisson's ratio of sweet cherry pit. The horizontal collision process of sweet cherry  
248 was accompanied by its own large deformation, so a large-displacement formulation was considered here when  
249 setting the collision analysis step in the simulation model. The duration of each collision was set to 10 ms, and  
250 the simulation analysis process was set to 100 analysis steps. Based on the selected high-accuracy sweet cherry  
251 horizontal collision FE model in Section 2.2, 18 horizontal collision FE simulations (3 temperature levels  $\times$   
252 2 collision types  $\times$  3 velocity levels) in Abaqus/explicit were performed based on an HP Z840 High-  
253 Performance Computer Platform with two E - 2683V4 16 - core 2.1 GHz Intel(R) CPUs and a 160 G DDR4 -  
254 2133 RegRAM. The detailed mechanical parameter setting in each simulation is shown in Table 1.

#### 255 **2.4 Post-processing analysis**

256 After the simulations were completed, the maximum Von mises stress, maximum impact force  $F_{max}$ , and  
257 collision damage volume of the fruit tissue during the collision process under different parameter conditions  
258 (environment temperature, initial velocity, collision type) were extracted from the output results. The collision  
259 damage volume was assessed via the approach described hereafter, which is similar to An et al. (2022). For the

260 sweet cherry collision simulation process, the stress change process of the integration points in the tissue  
 261 element was stored in the ODB file. A “Damage Analysis” post-processing plug-in in the Abaqus software was  
 262 secondary developed using Python language to access and read the stress changes of all the element integration  
 263 points of the exocarp and mesocarp tissue FE model during the entire collision simulation process. All the  
 264 elements of the fruit FE model were C3D10M with four integration points. Assuming that all elements were  
 265 regular tetrahedrons, and each integration point represents 1/4 of the volume of the entire tetrahedron. When  
 266 the stress value of an integration point in a tissue element was greater than the failure stress of the tissue, the  
 267 integration point was regarded as a failure integration point, and the failure volume of this element was 1/4 of  
 268 the whole element volume. After each collision simulation was completed, the Damage Analysis post-  
 269 processing plug-in was used to calculate the total number of failure integration points in the exocarp and  
 270 mesocarp model, respectively; and the SolidWorks software was used to extract the geometry model volume  
 271 of exocarp, mesocarp and pit, respectively. The sum of these three parts’ volumes was recorded as the total  
 272 fruit volume  $V_f$ . Equations (2) and (3) were used to calculate the damage volume of the exocarp and mesocarp  
 273 after each collision simulation, respectively. Equations (4) and (5) were used to calculate the percentage of the  
 274 damage volume of the exocarp and mesocarp, respectively.

$$275 \quad V_{\text{ex}} = \frac{1}{4} \times N_{\text{ex}} \times \frac{\sqrt{2}}{12} L_{\text{ex}}^3 \quad (2)$$

$$276 \quad V_{\text{me}} = \frac{1}{4} \times N_{\text{me}} \times \frac{\sqrt{2}}{12} L_{\text{me}}^3 \quad (3)$$

$$277 \quad P_{\text{ex}} = \frac{V_{\text{ex}}}{V_f} \times 100\% \quad (4)$$

$$278 \quad P_{\text{me}} = \frac{V_{\text{me}}}{V_f} \times 100\% \quad (5)$$

## 279 **2.5 Statistical analysis**

280 The multiple linear regression analysis was performed using SAS version 9.2 software (SAS Institute Inc.,  
 281 Cary, NC, USA), and the significance level was set at 0.05 ( $p = 0.05$ ). The maximum impact force, the fruit  
 282 damage volume and the percentage of damage volume were used as the collision damage degree indicators for  
 283 evaluating the susceptibility to collision damage of the sweet cherry fruit and were set as dependent variables.  
 284 Their potential influence factors, such as environment temperature, initial fruit velocity, and collision type,  
 285 were defined as independent variables. The collision type was a dummy variable, and its two levels, "fruit-to-  
 286 rigid surface collision type" and "fruit-to-fruit collision type" were coded as "0" and "1", respectively. The  
 287 environment temperature and the initial fruit velocity were quantitative variables.

## 288 **3. Results and discussion**

### 289 3.1. Validation of the fruit finite element model

290 Figure 1C shows the Von mises stress distribution contour of the exocarp, mesocarp and pit on the  
291 longitudinal equator section at the moment when the sweet cherry produced the maximum impact force during  
292 the horizontally collision with the rigid surface at the fruit initial velocity of 2.7 m/s. In this horizontal collision  
293 FE model, the elastic modulus, failure stress, Poisson's ratio and density of the sweet cherry's exocarp tissue  
294 were 2.10 MPa, 0.84 MPa, 0.40 and 1.01 g/cm<sup>3</sup>, the elastic modulus, failure stress, Poisson's ratio and density  
295 of the sweet cherry's mesocarp tissue were 0.30 MPa, 0.08 MPa, 0.37 and 1.05 g/cm<sup>3</sup>, and the elastic modulus,  
296 Poisson's ratio and density of the pit were 13000 MPa, 0.3 and 0.91 g/cm<sup>3</sup>, respectively. When the stress value  
297 of each tissue element exceeded its failure stress threshold, the element was presented as a gray failure element,  
298 that is, a damaged area. When the sweet cherry horizontally collided with the rigid surface at an initial velocity  
299 of 2.7 m/s, the maximum Von mises stress of exocarp and mesocarp tissue were 0.269 MPa and 0.313 MPa,  
300 respectively. The maximum stress value in exocarp FE model was much smaller than its tissue failure stress  
301 value, so the exocarp did not have any obvious damage during the horizontal collision at this velocity. However,  
302 the maximum stress value in the mesocarp FE model was greater than its tissue failure stress value, so the  
303 mesocarp had obvious damage during the horizontal collision process at this velocity, corresponding to the  
304 gray area in the tissue model.

305 Figure 1D shows the comparison between the simulation and the real experimental results when the sweet  
306 cherry horizontally collided with the rigid surface at a velocity of 2.7 m/s. Among them, the simulation 1,  
307 simulation 2 and simulation 3, respectively represent the simulation results when the elastic modulus and  
308 failure stress of the exocarp and mesocarp took the minimum, average and maximum measured values in the  
309 fruit FE model. These result parameters are the maximum impact force  $F_{max}$  of the fruit impacting on the rigid  
310 surface and the contact time  $T_c$  in the compression phase of the collision process. The experiment result  
311 presents the mean  $\pm$  standard deviation of two experimental result parameters. Compared with the experimental  
312 result, the relative errors of the maximum impact force of the fruit impacting on the rigid surface in the three  
313 simulation results were 11.3 %, 1.58 % and 4.76 %, and the relative errors of the contact time in the  
314 compression phase of the collision process were 3.04 %, 1.87 %, and 6.78 %, respectively. Therefore, when  
315 each tissue mechanical parameter took the average value in the fruit FE model, the relative error between the  
316 simulation and real experimental result was the smallest, and this fruit model would have a high prediction  
317 accuracy for dynamic collision behavior, so it would be used in the following sweet cherry collision damage  
318 analysis.

### 319 3.2 Damage evolution during the fruit-to-rigid surface and fruit-to-fruit collision processes

320 Figure 3-A1 and A2 show the Von mises stress distribution contour and the velocity distribution contour  
321 of the fruit in five motion states (0<sup>th</sup>, 15<sup>th</sup>, 30<sup>th</sup>, 45<sup>th</sup>, and 100<sup>th</sup> steps) in the fruit-to-rigid surface collision system  
322 ( $T = 20\text{ }^{\circ}\text{C}$ ,  $v = 2\text{ m/s}$ ), respectively. The 0<sup>th</sup> step is the initial state of the sweet cherry moving horizontally to  
323 the rigid surface at an initial velocity of 2 m/s. The 15<sup>th</sup> step represents a certain motion state of the sweet  
324 cherry in the compression phase of the collision process. At this step when the kinetic energy of the fruit was  
325 reduced, the kinetic energy was converted into the deformation energy inside the fruit, and the horizontal  
326 moving velocity of the sweet cherry acting on the rigid surface continued to decrease. The 30<sup>th</sup> step represents  
327 the moving state of the sweet cherry was at the maximum deformation, and the maximum contact stress  
328 occurred inside the fruit. The 45<sup>th</sup> step represents a certain motion state of the sweet cherry in the recovery  
329 phase of the collision process, the elastic deformation energy was converted into the kinetic energy of the fruit,  
330 and the horizontal moving velocity of the fruit was toward the left and continued to increase. The 100<sup>th</sup> step  
331 represents the motion state of the sweet cherry at 10 ms. Figures 3-A3, A4 and A5 show the Von mises stress  
332 distribution contour of the exocarp, mesocarp and pit on the fruit longitudinal equator section during the fruit-  
333 to-rigid surface collision process, respectively. Similarly, Figures 3-B1 and B2 show the Von mises stress  
334 distribution contour and the velocity distribution contour of the sweet cherry in five motion states (0<sup>th</sup>, 17<sup>th</sup>,  
335 34<sup>th</sup>, 51<sup>st</sup>, and 100<sup>th</sup> steps) in the fruit-to-fruit horizontal collision system ( $T = 20^{\circ}\text{C}$ ,  $v = 1\text{ m/s}$ ). In the fruit-to-  
336 fruit horizontal collision system, the sweet cherry fruit showed a similar motion state and energy conversion  
337 process to the fruit-to-rigid surface horizontal collision system at each step. The maximum Von mises stresses  
338 of the exocarp, mesocarp, and pit in the fruit-to-rigid surface collision process were larger than those in the  
339 fruit-to-fruit collision process (Fig. 3-A3, A4 and A5 and Fig. 3-B3, B4 and B5), and the damage area on the  
340 mesocarp model of the fruit-to-rigid surface collision process was larger than that of the fruit-to-fruit collision  
341 process (Fig. 3-A4 and Fig. 3-B4). This is due to the hardness difference between the two collision targets. The  
342 gray area in Fig. 3A and Fig. 3B represents the damaged area of the fruit. When the initial velocity of the fruit  
343 increased from 1 to 3 m/s and the environment temperature increased from 5  $^{\circ}\text{C}$  to 40  $^{\circ}\text{C}$ , no impact damage  
344 occurred in the sweet cherry exocarp, and the damage mainly occurred in the fruit mesocarp. This may be due  
345 to the fact that the exocarp tissue cells are small, dense, and have high toughness, which is difficult to be  
346 damaged during mild collision.

347 Figure 4A shows the internal damage evolution of fruit in the fruit-to-rigid surface horizontal collision  
348 process ( $v = 2\text{ m/s}$ ). Obviously, the damage did not occur instantaneously when the collision began but rather

349 after a certain time as the contact time increased. When the internal stress of the fruit accumulated to a certain  
350 level (that is, the failure stress of the tissue), the damage began to appear and continued to increase. According  
351 to the damage evolution curve (damage volume vs contact time), the impact damage volume of the fruit showed  
352 a nonlinear increase trend with the increase in the contact time, and in the later compression phase, the impact  
353 damage growth gradual slowed down, which may be related to the changing energy in the collision process.  
354 Studies have shown that internal damage of fruit is closely related to the absorption energy (An et al., 2020).  
355 According to the ALLKE curve of fruit kinetic energy vs contact time in the post-processing results, in the  
356 later compression phase, the rate of the reduction of the kinetic energy of the sweet cherry became slow, and  
357 the kinetic energy was mainly transferred into the internal deformation energy of the sweet cherry; that is, the  
358 absorption of energy by the fruit also led to the change of the internal stress of the fruit and caused the damage  
359 of the fruit tissue. The maximum damage volumes of sweet cherry in the fruit-to-rigid surface collision process  
360 at 5 °C, 20 °C and 40 °C were 115.79 mm<sup>3</sup>, 222.30 mm<sup>3</sup> and 328.83 mm<sup>3</sup>, respectively. Therefore, under the  
361 same initial fruit velocity, the impact damage degree of the sweet cherry increased with increasing temperature.  
362 Figure 4B shows the internal damage evolution of the sweet cherry in the fruit-to-fruit collision process. The  
363 trend of the internal damage evolution of the sweet cherry under the two collision types was basically similar,  
364 while their damage degree shows an obvious difference. The maximum impact damage volumes of sweet  
365 cherry in the fruit-to-fruit collision process at 5 °C, 20 °C and 40 °C were 32.70 mm<sup>3</sup>, 67.94 mm<sup>3</sup> and 98.67  
366 mm<sup>3</sup>, respectively.

### 367 **3.3 Sensitive of the fruit finite element model**

368 The mechanical parameters of the sweet cherry may affect the maximum impact force and contact time  
369 of the fruit acting on the rigid surface during the collision process. Figure 5A shows the impact force - contact  
370 time curves of the horizontal collision process between fruit and rigid surface when the elastic modulus and  
371 failure stress of the exocarp tissue and mesocarp tissue was average value at 20 °C ( $E_{ex} = 2.09$  MPa,  $\sigma_{ex} = 0.84$   
372 MPa,  $E_{me} = 0.30$  MPa,  $\sigma_{me} = 0.08$  MPa), increased by 20 % ( $E_{ex} = 2.51$  MPa,  $\sigma_{ex} = 1.00$  MPa,  $E_{me} = 0.36$  MPa,  
373  $\sigma_{me} = 0.10$  MPa), and decreased by 20 % ( $E_{ex} = 1.67$  MPa,  $\sigma_{ex} = 0.67$  MPa,  $E_{me} = 0.24$  MPa,  $\sigma_{me} = 0.07$  MPa),  
374 and the initial velocity of the fruit was all set to 2 m/s. The horizontal collision process between two objects  
375 included two phases: compression and recovery, which is similar to the viewpoint of apple collision proposed  
376 by Dintwa et al. (2008). In the compression phase, the impact force between the two objects increased  
377 nonlinearly with the increase of the collision contact time, and in the recovery phase, the impact force between  
378 the two objects decreased nonlinearly with the increase of the collision contact time. When the elastic-plastic

379 mechanical parameters of the sweet cherry tissue were inputted by its average values, the maximum impact  
380 force and contact time of the fruit acting on the rigid surface were 17.91 N and 5.0 ms, respectively. With the  
381 increase in the elastic modulus and failure stress of the sweet cherry tissue, the maximum impact force of the  
382 fruit acting on the rigid surface obviously increased while the contact time of the fruit acting on the rigid  
383 surface decreased. This result is not in agreement with that of two rigid bodies' collision. Figure 5B shows the  
384 impact force - contact time curves of the horizontal collision process between fruit and rigid surface when the  
385 plastic strains of the exocarp and mesocarp were 0.01, 0.02 and 0.03, respectively ( $E_{ex} = 2.09$  MPa,  $\sigma_{ex} = 0.84$   
386 MPa,  $E_{me} = 0.30$  MPa,  $\sigma_{me} = 0.08$  MPa,  $v = 2$  m/s). The results showed that the maximum impact force and  
387 contact time of the fruit acting on the rigid surface almost did not change with the increase in the plastic strain  
388 of the exocarp and mesocarp tissue.

389 The initial velocity of the fruit obviously affects the maximum impact force and contact time of the fruit  
390 acting on the rigid surface. Figure 5C shows the impact force - contact time curves of the horizontal collision  
391 process between fruit and rigid surface when the initial velocity of the fruit was 1 m/s, 2 m/s and 3 m/s,  
392 respectively. When the initial velocity of the fruit increased from 1 m/s to 3 m/s, the maximum impact force  
393 of the fruit acting on the rigid surface increased by 258.2 %, and the contact time decreased by 28.6 %. The  
394 curvature radius of the contact point on the fruit surface also affects the maximum impact force and contact  
395 time of the fruit acting on the rigid surface. Figure 5D shows the impact force - contact time curves of the  
396 horizontal collision process between fruit and rigid surface when the curvature radius of the contact point on  
397 fruit surface was 10.32 mm and 18.28 mm, respectively. When the curvature radius of the contact point on the  
398 fruit surface increased from 10.32 mm to 18.28 mm, the maximum impact force of the fruit acting on the rigid  
399 surface increased by 8.5 %, and the contact time of the fruit acting on the rigid surface decreased by 4.0 %.  
400 One possible explanation is that with the increase in the curvature radius of the contact point on the fruit surface,  
401 the collision area between the fruit and the rigid surface as well as the total force of the fruit tissue element  
402 nodes in the collision contact area increased, thereby the maximum impact force of the fruit acting on the rigid  
403 surface increased. Once the initial velocity  $v$  of the fruit is the same, the collision contact time will decrease  
404 under the condition of the conservation of momentum.

### 405 **3.4 Prediction of the collision-damage susceptibility of sweet cherry**

406 The results of the multiple linear regression analysis are listed by three Equations (6 - 8), which predicts  
407 the collision-damage susceptibility of the sweet cherry in the horizontal collision process with the maximum  
408 Von mises stress of fruit, the fruit damage volume, and the percentage of damage volume as dependent

409 variables, respectively. The three independent variables, namely collision type, initial fruit velocity, and  
410 environmental temperature, had significant effects on three dependent variables ( $p < 0.05$ ). From these  
411 regression equations, it can be seen that the collision type has the greatest effect on the damage susceptibility  
412 of the sweet cherry, followed by the initial fruit velocity and environmental temperature. The maximum stress,  
413 fruit damage volume and percentage of damage volume in the fruit-to-rigid surface collision type were 0.113  
414 MPa, 194.80 mm<sup>3</sup> and 1.72 % thus higher than those in the fruit-to-fruit collision type. The collisions between  
415 fruit and rigid surface and between fruit and fruit are the common collision type in the fruit postharvest  
416 handling. By contrast, it is found that the fruit is more easily damaged when it collides with a rigid surface  
417 when compared to the fruit-to-fruit collision at the same environmental temperature and initial fruit velocity.  
418 Similar results were reported in the research of the apple collision damage (Ahmadi et al., 2016). Different  
419 collision types include some potential hidden basic parameters that affect the degree of fruit collision damage,  
420 such as the surface curvature and the natural mechanical properties of the collided object (Yousefi et al., 2016;  
421 Zhou et al., 2016b).

422 Studies with the initial fruit velocity range of 1 m/s ~ 3 m/s, showed that when the initial velocity of sweet  
423 cherry increased by 1 m/s, the maximum Von mises stress inside the fruit increased by 0.051 MPa, the fruit  
424 damage volume increased by 143.49 mm<sup>3</sup> and the percentage of damage volume increased by 1.27 %. The  
425 magnitude of the initial velocity of the sweet cherry determines the magnitude of the momentum of the fruit  
426 before the horizontal collision to an object. The greater the initial velocity of the fruit, the greater are its  
427 momentum, the impulse of the sweet cherry to the collided object in a short time, and the maximum impact  
428 force of the fruit during the collision process. These results agree with those of Du et al. (2019) and Zhou et  
429 al. (2016b) showing that when the kiwifruit was dropped from the heights of 0.25 m, 0.50 m, and 1.0 m, the  
430 maximum stress of fruit was 2.082 MPa, 2.386 MPa, 3.101 MPa, and the fruit damage volume were 1878.4  
431 mm<sup>3</sup>, 4144.2 mm<sup>3</sup>, 10564.2 mm<sup>3</sup>, respectively (Du et al., 2019); and the drop height had a significant effect on  
432 the damage volume of sweet cherry (Zhou et al., 2016b). Different drop heights determined that sweet cherry  
433 had different initial velocities before the collision, and will produce different impact energies during the  
434 collision process. Moreover, there is a positive linear correlation between the fruit damage volume and the  
435 impact energy (An et al., 2022). Therefore, it is possible to reduce the collision-damage susceptibility of a fruit  
436 by lowering the initial vibration velocity of the fruit during postharvest handling.

437 In the temperature range of 5 °C ~ 40 °C, when the environmental temperature increased by 1 °C, the  
438 maximum Von mises stress inside the fruit during dynamic collision process decreased by 0.001 MPa, the fruit

439 damage volume increased by 4.09 mm<sup>3</sup>, and the percentage of damage volume increased by 0.04 %. The elastic  
440 modulus and failure stress of the sweet cherry showed a decreasing trend with the increase in environmental  
441 temperature (Han et al., 2022), so this could explain the decrease in the maximum stress of the fruit and the  
442 increase in the fruit damage volume and the percentage of damage volume during the horizontal collision of  
443 the sweet cherry with the increasing environmental temperature. Therefore, the mechanical properties of fruit  
444 biomaterials are also important indicators to judge the collision-damage susceptibility of fruit. Similar results  
445 were reported in the impact damage research of kiwifruit (Du et al., 2019).

$$446 \quad \sigma_{\max} = -0.113CT - 0.001T + 0.051v + 0.172 \quad R^2 = 0.97 \quad (6)$$

$$447 \quad V_{\text{fd}} = -194.80CT + 4.09T + 143.49v - 113.05 \quad R^2 = 0.78 \quad (7)$$

$$448 \quad P_{\text{fd}} = -1.72CT + 0.04T + 1.27v - 1.00 \quad R^2 = 0.78 \quad (8)$$

#### 449 **4. Conclusion**

450 A dynamic FE model was developed to quantitatively analyze the dynamic collision-damage susceptibility of  
451 sweet cherry under different environmental temperatures relevant to postharvest mechanical handling  
452 conditions. Also, a newly designed and built fruit-to-rigid surface horizontal collision testbed was used to  
453 experimentally validate the model. The average elastic moduli and failure stress of tissues were verified to be  
454 able to reproduce the maximum impact force and contact time in the compression stage of the fruit-to-rigid  
455 surface collision experiment. In the fruit-to-rigid surface and fruit-to-fruit collision processes, a nonlinear  
456 increasing relationship between fruit damage volume and collision contact time was observed. It was found  
457 that the maximum impact force and contact time were mainly sensitive to the elastic moduli and failure stress  
458 of tissues, initial fruit velocity, and curvature radius of the contact point at the fruit surface but were not  
459 sensitive to the tissue plastic strain during fruit-to-rigid surface collision simulation. Results of the multiple  
460 linear regression analysis showed that the collision type was the most important factor affecting the horizontal  
461 collision-damage susceptibility of the sweet cherry, followed by the initial fruit velocity and environmental  
462 temperature. Three obtained mathematical models can be used as a tool to quantitatively assess the degree of  
463 the internal damage of sweet cherry during grading, packaging, and transport for recommending  
464 improved handling methods in the supply chain. This study shows an effective numerical simulation approach  
465 for objectively predicting the horizontal collision-damage susceptibility of sweet cherry and other fresh fruit.

#### 466 **Acknowledgements**

467 This work was supported by a European Marie Curie International Incoming Fellowship (326847 and  
468 912847), a Chinese Universities Scientific Fund (2452018313) and an International Cooperation Key Plan of

469 Shaanxi Province (2022KWZ-12).

#### 470 **Author contributions**

471 X.H. designed the experiment, performed simulation and wrote the manuscript. Y.L., F.T., Z.L. and M.K.  
472 review and editing the manuscript. Z.L. and B.L. provided the resources support. X.H., Z.L. and B.L. provided  
473 calibration data. X.H., Y.L. and Z.L. designed the data visualization.

#### 474 **Declaration of competing interest**

475 The authors declare no competing interest.

#### 476 **References**

- 477 An, X., Li, Z., Zude-Sasse, M., Tchuenbou-Magaia, F., Yang, Y., 2020. Characterization of textural failure  
478 mechanics of strawberry fruit. *J. Food Eng.* 282, 110016. <https://doi.org/10.1016/j.jfoodeng.2020.110016>
- 479 An, X., Liu, H., Fadiji, T., Li, Z., Dimitrovski, D., 2022. Prediction of the temperature sensitivity of strawberry  
480 drop damage using dynamic finite element method. *Postharvest Biol. Technol.* 190, 111939.  
481 <https://doi.org/10.1016/j.postharvbio.2022.111939>
- 482 Ahmadi, E., Barikloo, H., Kashfi, M., 2016. Viscoelastic finite element analysis of the dynamic behavior of  
483 apple under impact loading with regard to its different layers. *Comput. Electron. Agric.* 121, 1-11.  
484 <https://doi.org/10.1016/j.compag.2015.11.017>
- 485 Alique, R., Zamorano, J., Martinez, M., Alonso, J., 2005. Effect of heat and cold treatments on respiratory  
486 metabolism and shelf-life of sweet cherry, type picota cv "Ambrunes". *Postharvest Biol. Technol.* 35(2),  
487 153-165. <https://doi.org/10.1016/j.postharvbio.2004.07.003>
- 488 Brueggenwirth, M., Fricke, H., Knoche, M., 2014. Biaxial tensile tests identify epidermis and hypodermis as  
489 the main structural elements of sweet cherry skin. *AoB Plants* 6, plu019. <https://doi.org/10.1093/aobpla/plu019>
- 491 Brüggewirth, M., Knoche, M., 2016. Factors affecting mechanical properties of the skin of sweet cherry fruit.  
492 *J. Am. Soc. Hortic. Sci.* 141, 45-53. <https://doi.org/10.21273/JASHS.141.1.45>
- 493 Celik, H., 2017. Determination of bruise susceptibility of pears to impact load by means of FEM-based explicit  
494 dynamics simulation. *Postharvest Biol. Technol.* 128, 83-97.  
495 <https://doi.org/10.1016/j.postharvbio.2017.01.015>
- 496 Celik, H., Rennie, A., Akinci, I., 2011. Deformation behaviour simulation of an apple under drop case by finite  
497 element method. *J. Food Eng.* 104(2), 293-298. <https://doi.org/10.1016/j.jfoodeng.2010.12.020>
- 498 Dintwa, E., Van Zeebroeck, M., Ramon, H., Tijssens, E., 2008. Finite element analysis of the dynamic collision

499 of apple fruit. *Postharvest Biol. Technol.* 49(2), 260-276. [https://doi.org/](https://doi.org/10.1016/j.postharvbio.2008.01.012)  
500 10.1016/j.postharvbio.2008.01.012

501 Du, D., Wang, B., Wang, J., Yao, F., Hong, X., 2019. Prediction of bruise susceptibility of harvested kiwifruit  
502 using finite element method. *Postharvest Biol. Technol.* 152, 36-44.  
503 <https://doi.org/10.1016/j.postharvbio.2019.02.013>

504 Gu, S., Xu, D., Zhou, F., Feng, K., Chen, C., Jiang, A., 2022. Repairing ability and mechanism of methyl  
505 jasmonate and salicylic acid on mechanically damaged sweet cherries. *Sci. Hortic.* 292, 110567.  
506 <https://doi.org/10.1016/j.scienta.2021.110567>

507 Han, X., An, X., Fadiji, T., Li, Z., Khojastehpour, M., 2022. Textural thermo-mechanical properties of sweet  
508 cherry for post-harvest damage analysis. *J. Texture Stud.* 53, 1-12. [https://doi.org/ 10.1111/jtxs.12661](https://doi.org/10.1111/jtxs.12661)

509 He, Y., Shi, J., 2009. Analysis and experiment on mechanical characteristic of walnut shell. *J. Xinjiang Agric.*  
510 *Univ.* 32(6), 70-75

511 Karatas, M., Arslan, N., 2016. Flow behaviours of cellulose and carboxymethyl cellulose from grapefruit peel.  
512 *Food Hydrocoll.* 58, 235-245. [https://doi.org/ 10.1016/j.foodhyd.2016.02.035](https://doi.org/10.1016/j.foodhyd.2016.02.035)

513 Li, Z., Li, P., Yang, H., Liu, J., 2013. Internal mechanical damage prediction in tomato compression using  
514 multiscale finite element models. *J. Food Eng.* 116(3), 639-647.  
515 <https://doi.org/10.1016/j.jfoodeng.2013.01.016>

516 Li, Z., Miao, F., Andrews, J., 2017. Mechanical models of compression and impact on fresh fruits. *Compr. Rev.*  
517 *Food Sci. F.* 16(6), 1296-1312. [https://doi.org/ 10.1111/1541-4337.12296](https://doi.org/10.1111/1541-4337.12296)

518 Mahiuddin, M., Godhani, D., Feng, L., Liu, F., Langrish, T., Karim, M., 2020. Application of caputo fractional  
519 rheological model to determine the viscoelastic and mechanical properties of fruit and vegetables.  
520 *Postharvest Biol. Technol.* 163, 111147. [https://doi.org/ 10.1016/j.postharvbio.2020.111147](https://doi.org/10.1016/j.postharvbio.2020.111147)

521 Michailidis, M., Karagiannis, E., Polychroniadou, C., Tanou, G., Karamanoli, K., Molassiotis, A., 2019.  
522 Metabolic features underlying the response of sweet cherry fruit to postharvest UV-C irradiation. *Plant*  
523 *Physiol. Biochem.* 144, 49-57. <https://doi.org/10.1016/j.plaphy.2019.09.030>

524 Miraei Ashtiani, S., Sadrnia, H., Mohammadinezhad, H., Aghkhani, M., Khojastehpour, M., Abbaspour-Fard,  
525 M., 2019. FEM-based simulation of the mechanical behavior of grapefruit under compressive loading.  
526 *Sci. Hortic.* 245, 39-46. <https://doi.org/10.1016/j.scienta.2018.10.006>

527 Namdari Gharaghani, B., Maghsoudi, H., 2018. Free fall analysis of orange fruit using numerical and  
528 experimental methods. *Int. J. Food Prop.* 21(1), 484-495. <https://doi.org/>

529 10.1080/10942912.2018.1446148

530 Nikara, S., Ahmadi, E., Alavi Nia, A., 2020. Finite element simulation of the micromechanical changes of the  
531 tissue and cells of potato response to impact test during storage by scanning electron microscopy.  
532 *Postharvest Biol. Technol.* 164, 111153. <https://doi.org/10.1016/j.postharvbio.2020.111153>

533 Pieczywek, P., Zdunek, A., 2014. Finite element modelling of the mechanical behaviour of onion epidermis  
534 with incorporation of nonlinear properties of cell walls and real tissue geometry. *J. Food Eng.* 123, 50-59.  
535 <https://doi.org/10.1016/j.jfoodeng.2013.09.012>

536 Pullanagari, R., Li, M., 2021. Uncertainty assessment for firmness and total soluble solids of sweet cherries  
537 using hyperspectral imaging and multivariate statistics. *J. Food Eng.* 289, 110177.  
538 <https://doi.org/10.1016/j.jfoodeng.2020.110177>

539 Salarikia, A., Miraei Ashtiani, S., Golzarian, M., Mohammadinezhad, H., 2017. Finite element analysis of the  
540 dynamic behavior of pear under impact loading. *Inf. Process. Agric.* 4(1), 64-77.  
541 <https://doi.org/10.1016/j.inpa.2016.12.003>

542 Wang, Y., Long, L., 2014. Respiration and quality responses of sweet cherry to different atmospheres during  
543 cold storage and shipping. *Postharvest Biol. Technol.* 92, 62-69. <https://doi.org/10.1016/j.postharvbio.2014.01.003>

544

545 Wang, Y., Zhang, Y., Yang, Y., Zhao, H., Yang, C., He, Y., Wang, K., Liu, D., Xu, H., 2020. Discrete element  
546 modelling of citrus fruit stalks and its verification. *Biosyst. Eng.* 200, 400-414.  
547 <https://doi.org/10.1016/j.biosystemseng.2020.10.020>

548 Wu, S., Gu, L. 2012. Introduction to the explicit finite element method for nonlinear transient dynamics. Wiley.  
549 <https://doi.org/10.1002/9781118382011>

550 Yamazaki, A., Hosokawa, M., 2019. Increased percentage of fruit set of F-1 hybrid of *Capsicum chinense*  
551 during high-temperature period. *Sci. Hortic.* 243, 421-427. <https://doi.org/10.1016/j.scienta.2018.08.049>

552 Yousefi, S., Farsi, H., Kheiralipour, K., 2016. Drop test of pear fruit: experimental measurement and finite  
553 element modelling. *Biosyst. Eng.* 147, 17-25. <https://doi.org/10.1016/j.biosystemseng.2016.03.004>

554 Zhao, H., Fu, M., Du, Y., Sun, F., Chen, Q., Jin, T., Zhang, Q., Liu, B., 2021. Improvement of fruit quality and  
555 pedicel color of cold stored sweet cherry in response to pre-storage 1-methylcyclopropene and chlorine  
556 dioxide treatments: combination treatment of 1-MCP plus ClO<sub>2</sub> improves post-harvest quality of sweet  
557 cherry fruit. *Sci. Hortic.* 277, 109806. <https://doi.org/10.1016/j.scienta.2020.109806>

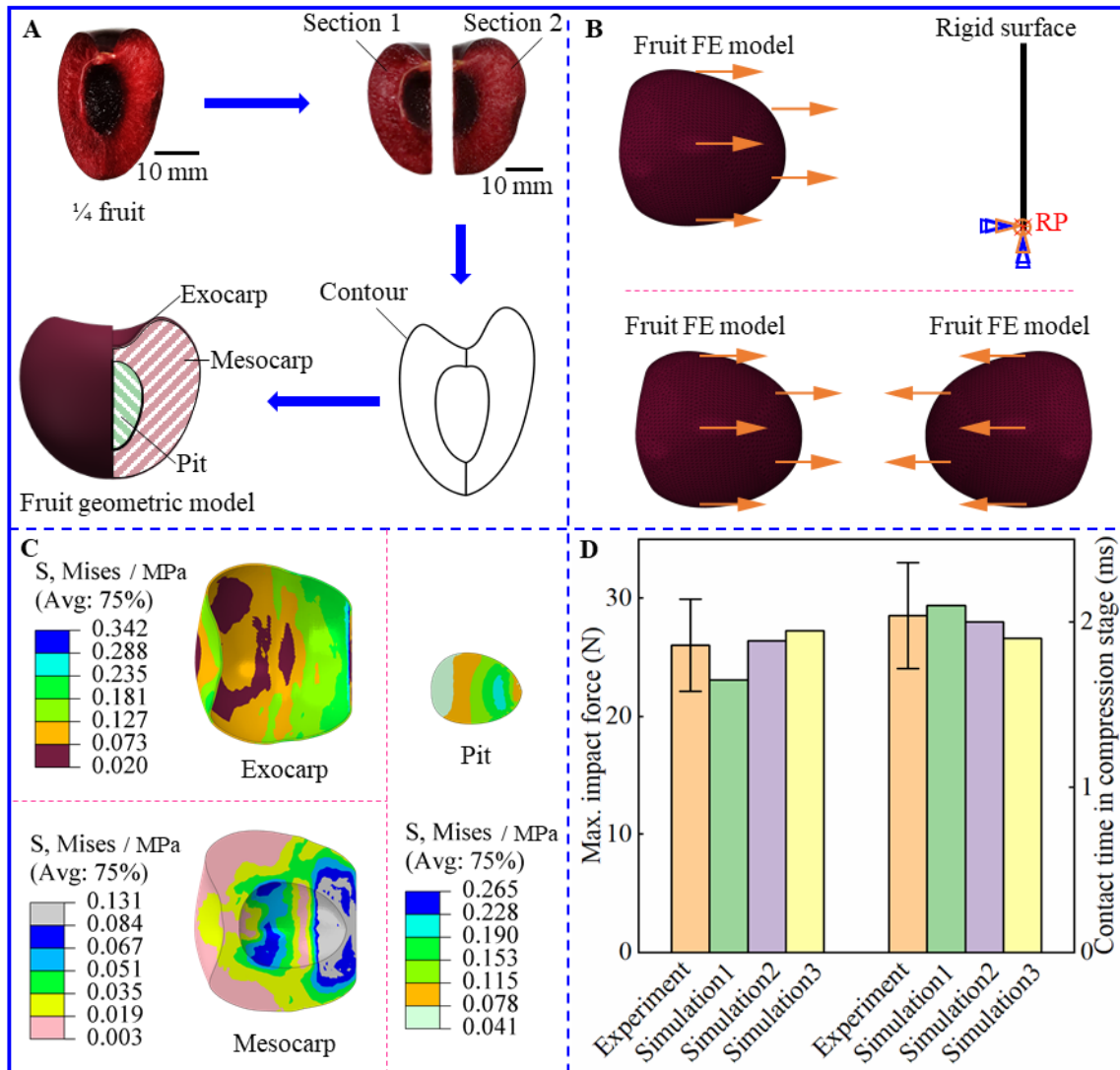
558 Zhao, H., Liu, B., Zhang, W., Cao, J., Jiang, W., 2019. Enhancement of quality and antioxidant metabolism of

559 sweet cherry fruit by near-freezing temperature storage. *Postharvest Biol. Technol.* 147, 113-122.  
560 <https://doi.org/10.1016/j.postharvbio.2018.09.013>

561 Zhou, J., He, L., Karkee, M., Zhang, Q., 2016a. Analysis of shaking-induced cherry fruit motion and damage.  
562 *Biosyst. Eng.* 144, 105-114. <https://doi.org/10.1016/j.biosystemseng.2016.02.007>

563 Zhou, J., He, L., Karkee, M., Zhang, Q., 2016b. Effect of catching surface and tilt angle on bruise damage of  
564 sweet cherry due to mechanical impact. *Comput. Electron. Agric.* 121, 282-289.  
565 <https://doi.org/10.1016/j.compag.2016.01.004>

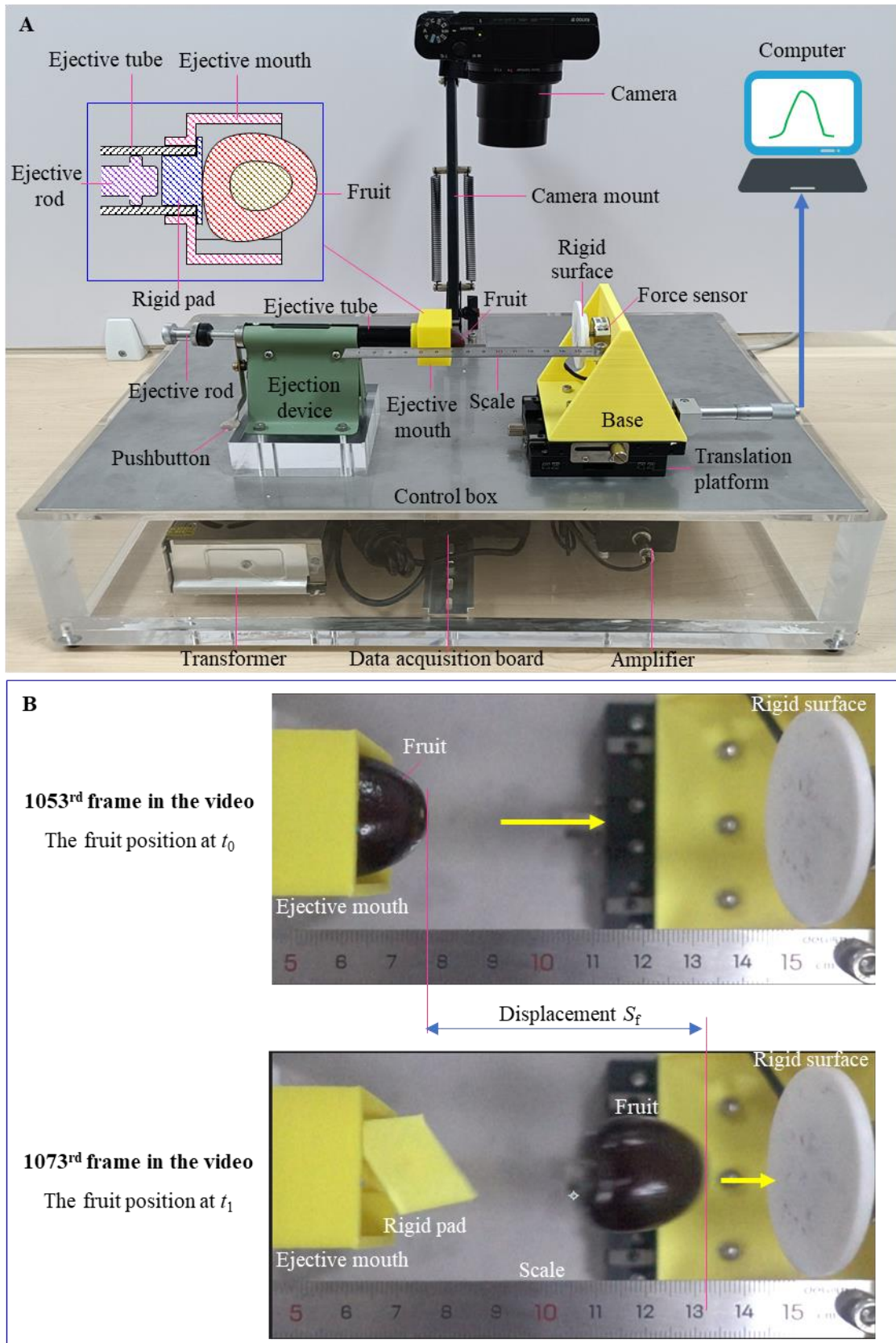
566 Zulkifli, N., Hashim, N., Harith, H., Mohamad Shukery, M., 2020. Finite element modelling for fruit stress  
567 analysis - a review. *Trends Food Sci. Technol.* 97, 29-37. <https://doi.org/10.1016/j.tifs.2019.12.029>  
568



571

572 **Fig. 1** Finite element modeling and simulation of two collision systems. (A) fruit geometric modeling, (B)  
 573 finite element modeling of two horizontal collision systems, (C) stress distribution contour of exocarp,  
 574 mesocarp and pit on the longitudinal equator section of fruit model at the moment of the maximum fruit  
 575 deformation, (D) the maximum impact force and contact time in collision experiment and simulations,  
 576 Simulation 1, 2 and 3 refers to the results of three simulations inputted by the minimum, average and maximum  
 577 measured elastic modulus and failure stress of exocarp and mesocarp, respectively.

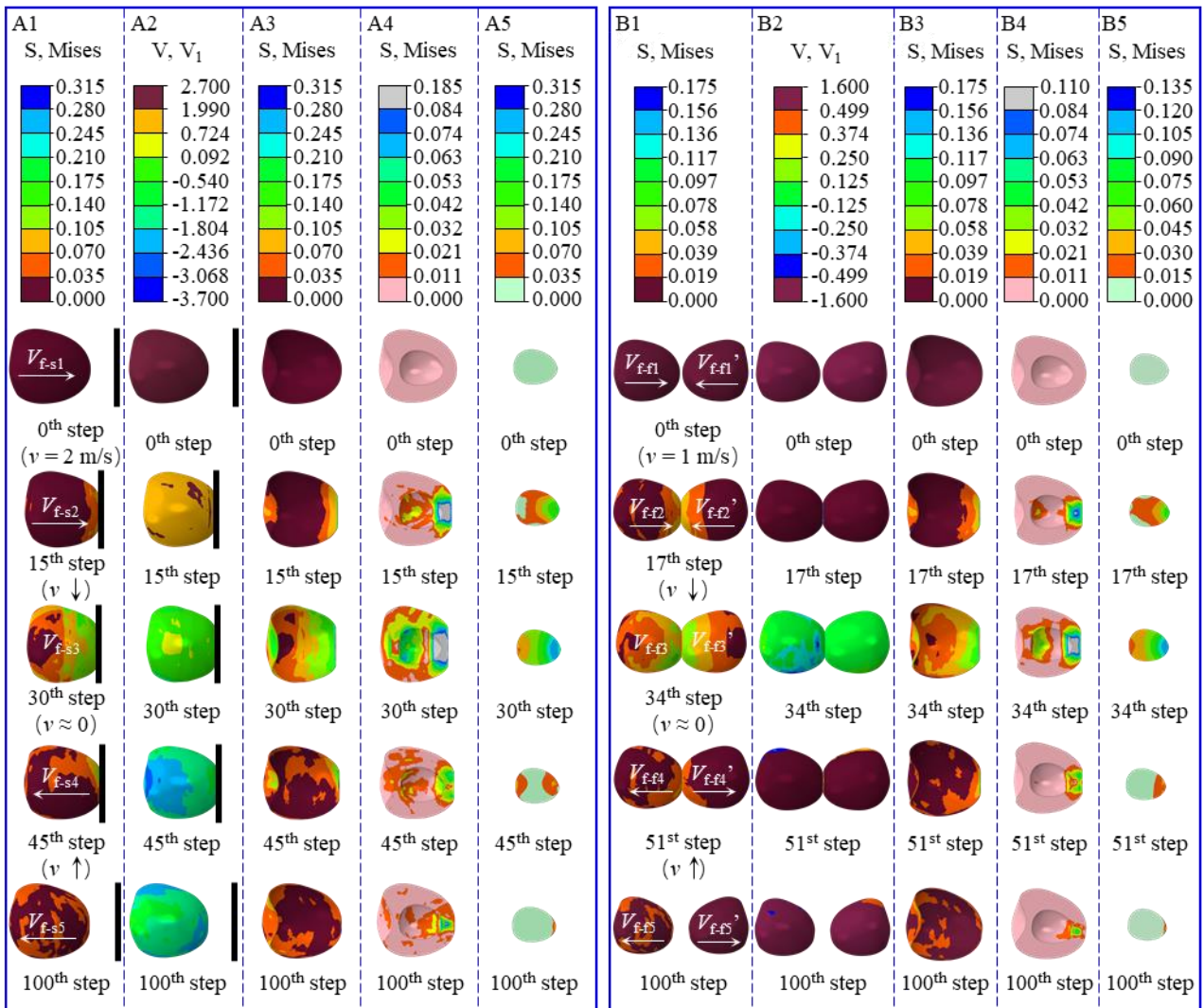
578



580

581 **Fig.2** Fruit-to-rigid surface horizontal collision experiment. (A) the fruit-to-rigid surface horizontal collision

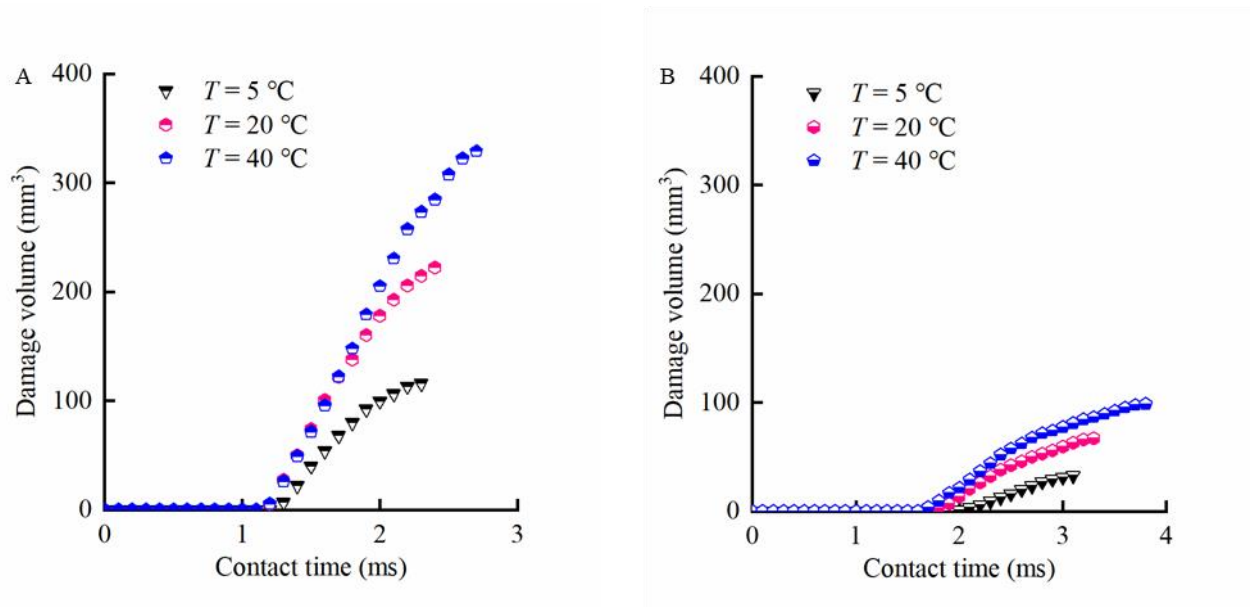
582 test device, (B) the moving process of a fruit in the horizontal collision test video.



586 **Fig. 3** Two types of horizontal collision processes. (A1, A2) Von mises stress distribution contour and velocity  
 587 distribution contour of whole fruit in the fruit-to-rigid surface collision process, respectively; (A3, A4, A5)  
 588 Von mises stress distribution contour of exocarp, mesocarp and pit in the fruit-to-rigid surface collision process,  
 589 respectively; (B1, B2) Von mises stress distribution contour and velocity distribution contour of whole fruit in  
 590 the fruit-to-fruit collision process, respectively; (B3, B4, B5) Von mises stress distribution contour of exocarp,  
 591 mesocarp and pit in the fruit-to-fruit collision process, respectively.

593 **Figure 4**

594



595

596 **Fig. 4** Damage evolution process of sweet cherry. (A) Damage volume vs Contact time of sweet cherry in the

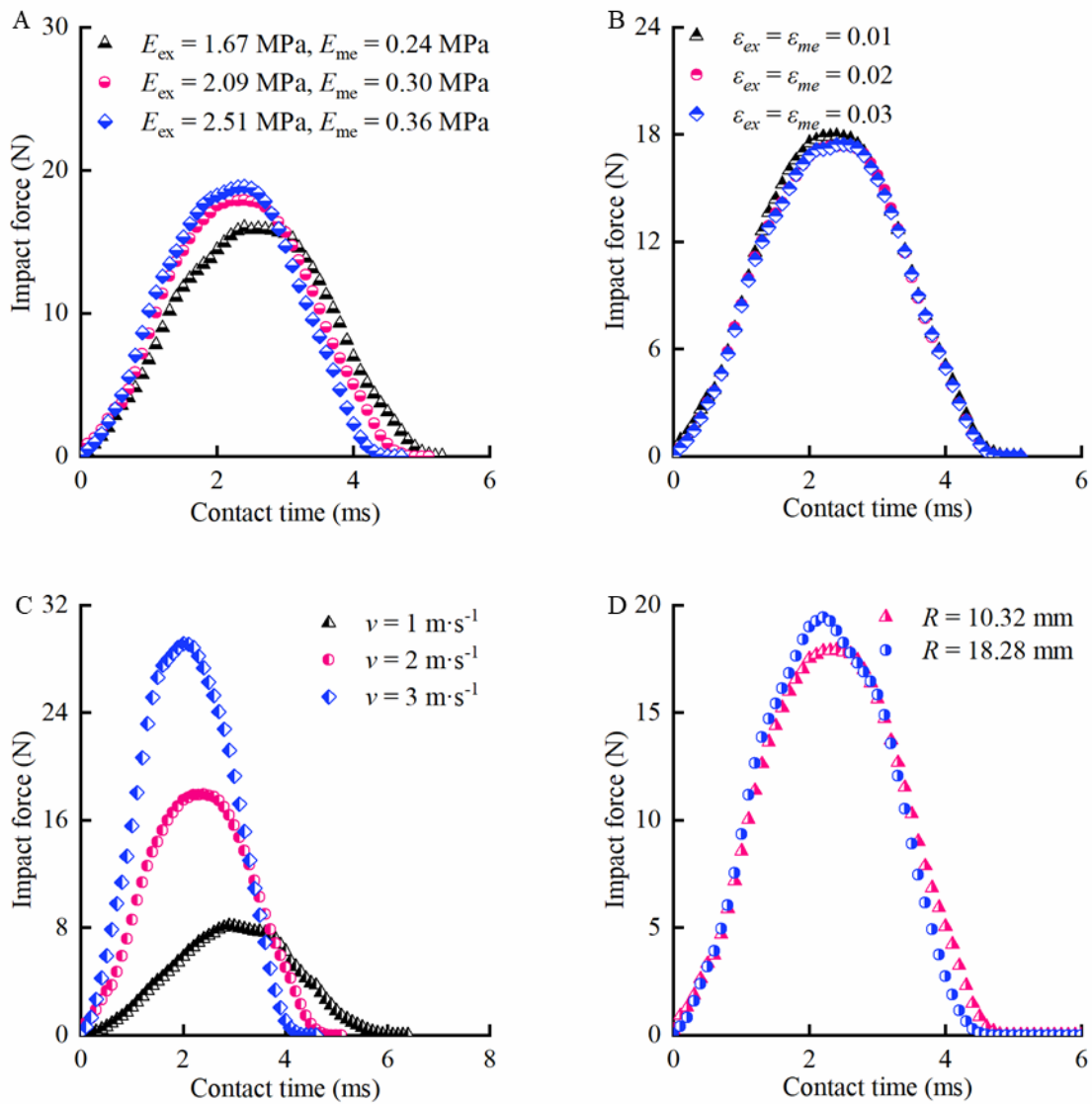
597 fruit-to-rigid surface collision process ( $T$  – environmental temperature), (B) Damage volume vs Contact time

598 of sweet cherry in the fruit-to-fruit collision process

599

600 **Figure 5**

601



602

603 **Fig. 5** Sensitive analysis of the fruit FE model. (A) Sensitive of the fruit FE model to tissue elastic modulus,

604 (B) Sensitive of the fruit FE model to tissue plastic strain, (C) Sensitive of the fruit FE model to initial fruit

605 velocity, (D) Sensitive of the fruit FE model to curvature radius.

606

607 **Table 1**

608

609 **Table 1** Mechanical parameters of fruit tissues and rigid surface in the 3D collision FE model

No. of simulation	Temperature (°C)	Collision type	Velocity (m/s)	Mechanical and physical parameters	
				Temperature-independent parameters	Temperature-dependent parameters
1	5	Fruit vs Rigid surface	1	$\rho_{ex} = 1.01$	$E_{ex} = 2.28 \pm 0.25$
2			$\rho_{me} = 1.05$	$E_{me} = 0.33 \pm 0.03$	
3			$\rho_p = 0.92$	$\sigma_{ex} = 0.89 \pm 0.13$	
4		Fruit vs Fruit	0.5	$E_p = 13000$	$\sigma_{me} = 0.11 \pm 0.01$
5			1	(He and Shi, 2009)	(Han et al., 2022)
6			1.5	$v_{ex} = 0.40$	
7	20	Fruit vs Rigid surface	1	$v_{me} = 0.37$	$E_{ex} = 2.10 \pm 0.25$
8			2	(Mahiuddin et al., 2020)	$E_{me} = 0.30 \pm 0.02$
9			3	$v_p = 0.30$	$\sigma_{ex} = 0.84 \pm 0.25$
10		Fruit vs Fruit	0.5	(He and Shi, 2009)	$\sigma_{me} = 0.08 \pm 0.01$
11			1	$E_{tex} = E_{tme} = 0.30$	(Han et al., 2022)
12			1.5	(Du et al., 2019)	
13	40	Fruit vs Rigid surface	1		$E_{ex} = 1.72 \pm 0.17$
14			2		$E_{me} = 0.22 \pm 0.02$
15			3		$\sigma_{ex} = 0.81 \pm 0.14$
16		Fruit vs Fruit	0.5		$\sigma_{me} = 0.06 \pm 0.01$
17			1		(Han et al., 2022)
18			1.5		

610